Granular Matter (2014) 16:185–191
DOI 10.1007/s10035-013-0474-0

ORIGINAL PAPER

Experimental measurements of orientation and rotation of dense 3D packings of spheres

Matt Harrington · Michael Lin · Kerstin N. Nordstrom · Wolfgang Losert

Received: 5 August 2013 / Published online: 7 January 2014

Abstract Many recent advances in the study of granular media have stemmed from the improved capability to image and track individual grains in two and three dimensions. While two-dimensional systems readily yield both translational and rotational motion, a challenge in three-dimensional experiments is the tracking of rotational motion of isotropic particles. We propose an extension of the refractive index matched scanning technique as a method of measuring individual particle rotation. Initial measurements indicate that shear-driven rotational motion may stem from gear-like motion within the shear zone.

Keywords Rotational motion · Three-dimensional imaging · Shear-banding · Particle tracking · Friction

1 Introduction

Current experimental research on dense granular flows has placed a heavy interest in the quantification of individual grain motion. Details of the microscopic origins of granular motion are typically lost in bulk rheological measurements, but researchers now have rigorous imaging techniques for acquiring particle-scale dynamics at their disposal. In particular, capturing the motion of grains inside a three-dimensional (3D) system is a challenge that has been addressed with techniques such as X-ray tomography [1], magnetic resonance imaging (MRI) [2], confocal microscopy [3], and refractive index matched scanning (RIMS) [4]. These techniques have provided additional insight to local structure, both static [5–7] and dynamically evolving under driving forces [8–13], velocity profiles [2,14–18], reversibility [19], size segregation [20–22], and response to impact [23]. All of these methods capture the translational motion of grains, which is often sufficient in the appropriate context. However, granular materials consist of particles large enough to be considered athermal [24], so every grain should be thought of as a solid body that exhibits an orientation that may change over time under the mechanics of rigid body motion.

Consider a collection of hard grains in a system of dimensionality D, which dictates the number of degrees of freedom accessible for translation, D, and rotation, $\frac{D(D-1)}{2}$. A pair of grains in contact mutually exert a normal repulsive contact force on each other, as well as a tangential frictional force at the grain surface. Each one of those grains is likely touching other grains as well, so it feels additional normal and tangential forces from those contacts. The sum of the tangential forces yields a net torque on the individual grain, which can lead to rotational acceleration when torques are unbalanced, or static rotational equilibrium when torques are balanced.

Measurements of individual grain rotation have been made in some previous work, but much of the recent formal discussion is limited to rotations within a granular gaseous state. For example, the internal energy of a real 2D driven dense gas has equal contributions from each degree of freedom in rotational and translational motion [25]. Equipartition is not generally observed in 3D dilute gases [26], but linear velocity vectors and particle rotation axes are correlated [27]. Whether equipartition is broken by density or dimensionality is not immediately clear. There are also observations from simulations that indicate the prevalence of rotations in

M. Harrington (✉) · M. Lin · K. N. Nordstrom
Department of Physics and IREAP, University of Maryland, College Park, MD 20742, USA
e-mail: mjharrin@umd.edu

W. Losert
Department of Physics, IPST, and IREAP, University of Maryland, College Park, MD20742, USA
e-mail: wlosert@umd.edu

the shear-banding of a dense system. The presence of inter-particle friction can affect the geometry of shear-bands under a biaxial load [28,29] and split-bottom shear [30], indicating that energy is either dissipated through sliding contacts or stored as rotational energy within rolling subregions [28,31]. The observation of rotational motion within the shear band of a real biaxial load predates simulations [32], while particle rotations in the shear zone of a split-bottom geometry has been recently verified in the alignment of rod-like particles [12,13,33]. However, the relative contributions of particle rotations and frictional dissipation in the formation of split-bottom shear zones have not been formally studied.

Measuring 3D orientation and rotational motion in real systems brings about additional challenges, particularly for dense systems of spherical grains. Unlike rods, solid spheres do not have an intrinsic orientation that arises from geometric asymmetry, so the orientation is indiscernible by current 3D imaging techniques. In this paper, we propose and demonstrate a technique for extracting spherical grain orientations and a portion of their rotational motion in a dense 3D system. Then, we report on the performance quality of our orientation algorithm in initial experiments. Finally, we connect the bulk particle rotation profiles with well-known azimuthal velocity profiles in the split-bottom geometry. This provides an indication of the origin of individual rotational motion in a system driven by circular shear.

2 Setup and procedure

2.1 Granular system

The dense granular pile ($\phi = 0.60 \pm 0.01$) is comprised of 6 mm polymethyl methacrylate spheres, each of which has a 1.5 mm diameter hole drilled all the way through (see Fig. 1). The cylindrical hole through the sphere introduces a slight inertial anisotropy of $\frac{I_{2,3}}{I_1} = 0.929$ (see "Appendix").

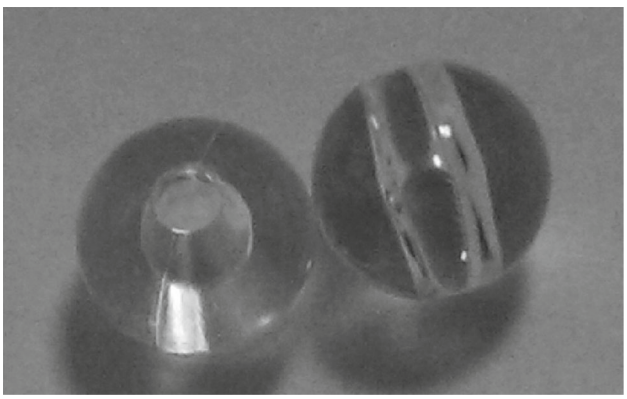

Fig. 1 Photograph of the drilled beads used for capturing rotational motion

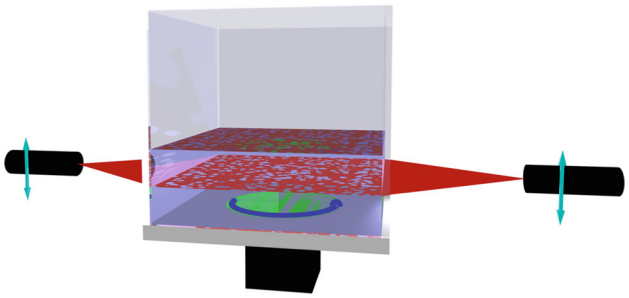

Fig. 2 Illustration of the shear cell, with index-matching fluid and 3D imaging apparatus. A camera that captures *horizontal* cross-sections from the *top-down* is not shown

The grains are placed in a circular split-bottom shear geometry, illustrated in Fig. 2. This geometry is known for producing wide shear zones [34,35], and has recently been used for studying rotational motion and ordering of anisotropic particles [12]. The square tank has side lengths of 15 cm and the shearing disk diameter is 9 cm. The disk is separate from the tank floor and rotates at a rate of 1 mrad/s, either steadily or in an oscillatory fashion. The results shown in this paper are derived from 2 full rotations of steady shear. The average pile height is selected to be about 4.5 cm, so the height to disk radius ratio $\frac{H}{R_s} \approx 1$. This is the same setup used previously in several studies examining shear-driven granular flow in 3D [11,17,19,22]. Before any data is collected, we pour the grains into the tank and shear steadily for 2 full disk rotations to eliminate any fabric memory from the initial loading of the packing.

2.2 Acquisition of 3D images

The grains are immersed in a fluorescent index-matched fluid, Triton X-100 with Nile Blue 690 Perchlorate. A small amount of hydrochloric acid is also added to stabilize the mixture. The density of the grains ($\rho_g = 1.18$ g/cm^3) is greater than that of the fluid ($\rho_f = 1.07$ g/cm^3), so the grains settle at the bottom of the tank under gravity. Although the system is fluid-immersed, the flows observed under our choice of shearing rate (1 mrad/s) are rate-independent, as well as similar to those of a dry pile [17].

Cross sections within the pile are illuminated by two laser sheets (635 nm) which are aligned on opposite sides of the tank, as shown in Fig. 2. A high-sensitivity camera then captures an image of the horizontal cross section from the top down. The laser sheets scan vertically through the entire pile, in 200 μm steps, to capture a full 3D image. This imaging procedure is repeated between 2° increments in shear.

Typical cross sections using solid and drilled grains are shown in Fig. 3. Note that both images yield circular cross-sections of each individual grain, while the cavities in the drilled grains are clearly visible.

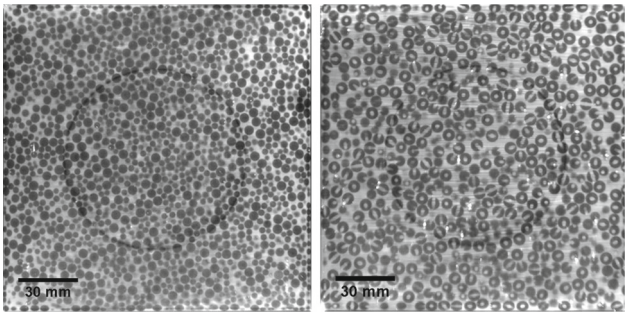

Fig. 3 (*Left*) A cross section within the bidisperse system used in Harrington et al. [22], which contains *solid spheres* of size $D_S = 3.2$ mm and $D_L = 4.8$ mm. (*Right*) A cross section of the pile with drilled grains, $D = 6$ mm and hole diameter 1.5 mm

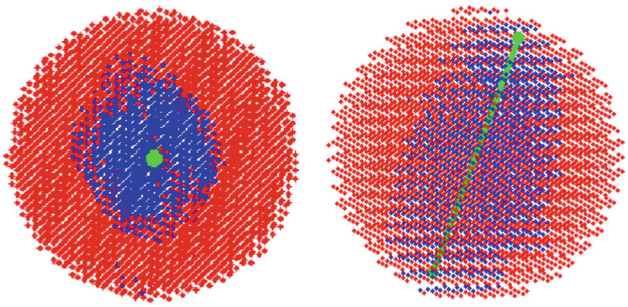

Fig. 4 Two views of the orientation extraction of a single grain

2.3 Particle extraction

The locations of individual grain centroids are obtained by applying a 3D Gaussian convolution kernel [36]. Since the kernel primarily detects the edge of spheres to determine centroid location, the positions of drilled spheres are not significantly affected compared to solid spheres.

In the case of drilled beads, the presence of a cavity allows us to then extract particle orientations. Once the centroid of a grain is determined, a spherical neighborhood surrounding the centroid, with a radius slightly smaller than the grain radius, is isolated. Principal component analysis (PCA) is then performed on bright pixels that correspond to the hole, leaving out dark pixels that represent the solid portion. The grain orientation vector is given by the eigenvector associated with the maximum eigenvalue of the covariance matrix, which is defined by the spread of bright band pixels in 3D space. A binary 3D image of a single grain with an extracted orientation using this method is shown in Fig. 4.

2.4 Tracking translational and rotational motion

Individual grains are identified and tracked in 3D using Particle Tracking Velocimetry [37]. This and other tracking algorithms uniquely label each particle and determine the translational motion. Next, the change in orientation axis between consecutive frames is directly calculated for every tracked grain. An additional check on the angular displacement is performed to avoid overestimating the rotational motion. This kind of error can result if PCA yields orientation vectors in consecutive frames that point in nearly opposite directions.

It is important to now emphasize that, while this PCA method is sufficient to capture two rotational degrees of freedom, there is an additional degree of freedom along the axis of the drilled hole that cannot be measured.

3 Results

3.1 Extraction performance

As stated previously, the presence of the cylindrical hole does not significantly affect grain position. Using ordinary solid spheres, particle center resolution is typically about 100 μm, which is consistent with the drilled grains. Furthermore, the orientations of stationary grains far from the disk are seen to fluctuate within a total angular deflection of 1 mrad (0.06°).

In a given frame, both positions and orientations can be found for at least 90 % of the grains, a slightly lower success rate from prior studies using solid spheres. In some cases, the position of a grain can be found, while the grain cavity is not adequately resolved to definitively assign an orientation. This effect is caused by the presence of additional solid-fluid interfaces, which further amplifies image distortion due to any disparity in the indices of refraction. The current success rate provides a very good basis to examine initial bulk measurements of rotations throughout the pile. In the future, however, we would like to capture an even higher percentage of grain orientations and rotations under improved index-matching. Then, reliable measurements of rotational motion within neighborhoods can be taken and reported.

Sample images depicting our extraction and tracking capabilities are shown in Fig. 5. Notice in the track image (right side of Fig. 5) how some grains maintain a very consistent orientation, while others rotate very quickly. Some grains even maintain consistent orientations for several frames, followed by intermittent rotations.

At this point, one aspect of our drilled spheres that should be addressed is the possibility of grains touching each other at the small cavity created by the drill hole. Figure 6a–b demonstrate two general ways that two grains can come into contact: (1) as with any solid sphere contact, the spherical surfaces of the grains are in contact with each other, and (2) the points of contact actually lie on the lip of the drill hole, such that the surface of one grain slightly penetrates the drill hole cavity of the other. Grains that are in contact under the latter condition are what we refer to as "sticking". To address this issue, we measure the probability density of the angle ϕ between a grain's orientation and the relative position

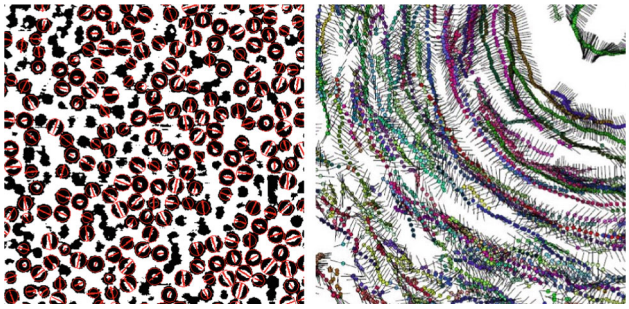

Fig. 5 (*Left*) Grain positions and orientations overlaid over a binary cross section of the pile, after processing. This image corresponds to a height of 1.5 cm and a 10 cm × 10 cm area centered about the shearing disk. *Circular outlines* are drawn around extracted grain positions, while the lines are projections of the orientation vector. *Dark circles* with lines laid across indicate nearly horizontally oriented grains, with the cavity lying just out of plane. (*Right*) Several sample trajectories passing through a height of 1.5 cm within a 3.0 cm × 2.9 cm area. The *small circles* are centroids, while the lines protruding from them are the grain cavity orientations. The *colors* indicate distinct tracks. The *top right corner* corresponds to the disk center

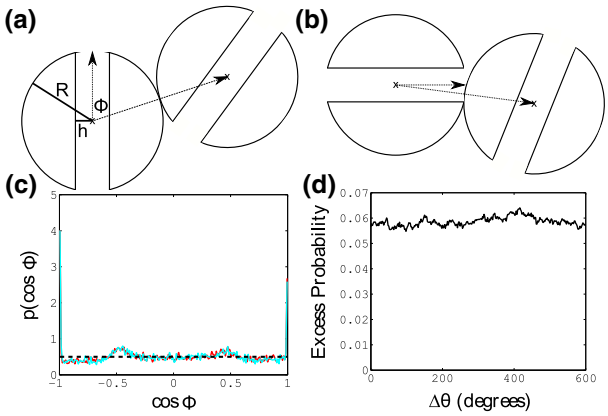

Fig. 6 **a** A cross sectional view of two drilled spheres whose contact point lies entirely on the grain surface. R is the grain radius, h is the drill hole radius, and ϕ is the angle between the orientation axis of one grain and the relative position vector between the two grains. **b** Two "sticking" grains whose points of contact are on the edge of the drill hole. **c** The probability density of $\cos\phi$ at an initial distribution (*dark red*) and after 600° of strain (*light cyan*), which mostly overlap each other. For reference, a perfectly uniform distribution is also shown (*dotted black*). **d** Over the course of 600° of strain, the probability of a grain contact sticking, in excess of the ideal uniform case

vector to its neighbor contacts. For sticking contacts, these vectors are very close to being either parallel or antiparallel. Specifically, a sticking contact is defined as one in which $|\cos\phi| \geq \frac{R}{\sqrt{R^2+h^2}}$, where R is the grain radius and h is the hole radius. This condition also includes the particular case where the orientations of both grains and the points of contact in between are all aligned. For the grains used in this study, this limit is found to be $|\cos\phi| \geq 0.97$. Figure 6c illustrates that a bias does indeed exist for sticking contacts at any given time, while much of the distribution in between remains close to uniform. However, the distribution does not change over large values of strain. In fact, Fig. 6d illustrates that the magnitude of the bias does not vary appreciably. Rather than driving the grains into a locked arrangement, the system exhibits a steady amount of sticking contacts which are not intrinsically preferred or stable. We also observe that sticking contacts that persist throughout the entirety of the experiment lie in an immobile region of the tank, far from the disk center.

3.2 Rotational coupling with velocity profiles

Given our capability to track grains in both space and orientation, we would now like to quantify the resulting velocity profiles, as well as the average rotation within several portions of the pile. As with previous experiments in circular split-bottom geometries, the grains exhibit azimuthal velocity profiles, as a function of r at fixed z, in the form of error functions [34,35]. As a result, the corresponding velocity gradient is sharply peaked in the middle of what is determined to be the shear zone. The shear zone is the intermediate region that separates two contrasting regions: one near the center of disk where grains undergo solid-body rotation, and a stationary region far from the disk center. The center of the shear zone moves slightly toward the disk center and the shear zone widens with increasing z. Figure 7a demonstrates the behavior of the azimuthal velocity, as well as the corresponding gradients in tangential velocity.

Strikingly similar behavior is then seen in the average θ-rotation of individual grains (that is, the z-component of particle angular velocity, ω_z). As shown in Fig. 7b, ω_z peaks at approximately the same locations in r and z as the tangential velocity gradient, and exhibits a width that is similar to that of the shear zone. This suggests that the gradients in tangential velocity may be what is directly driving ω_z.

In fact, a relationship between azimuthal rotation and tangential velocity gradient can be derived using only elementary mechanics, under special conditions. Consider the physical system illustrated in Fig. 8. A sphere of radius R is wedged between two plates which are aligned and parallel. The plates are located at perpendicular distances of r_1 and r_2 from a reference origin. If the plates translate at different velocities, v_1 and v_2, and the sphere does not slip between either of the plates, it will rotate instantaneously along an axis perpendicular to r_i and v_i. The amount of rotation is

$$\omega = \frac{v_2 - v_1}{R} = \frac{\Delta v}{R}$$

The tangential velocities of the plates can also be written in terms of angular velocities relative to the origin, $v_i = r_i \Omega_i$. Also, the sphere radius can be substituted with the plate

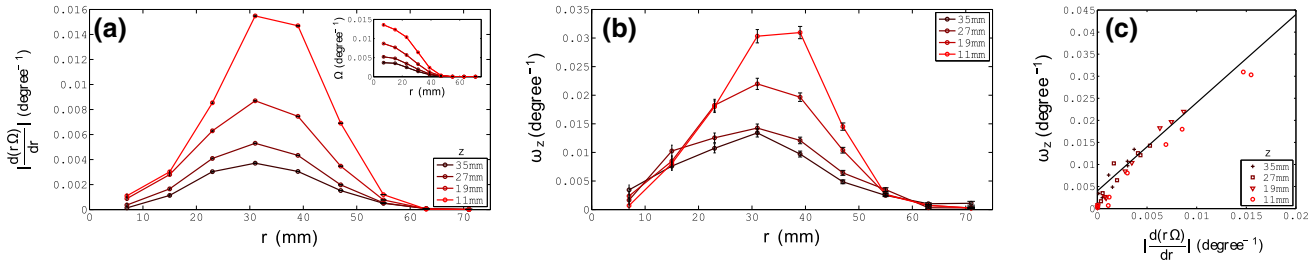

Fig. 7 (**a**, *Inset*) Azimuthal velocity (Ω) profiles within the pile as a function of r for various heights in z. (**a**, Main) The gradient of tangential velocity, $r\Omega$, with respect to r. **b** The average z-component of rotational motion (ω_z) as a function of r at various heights in z. **c** ω_z versus tangential velocity gradient. The *solid black line* has slope 2, as prescribed in Eq. 1

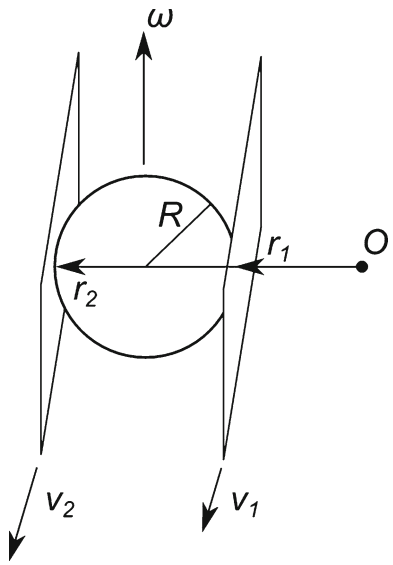

Fig. 8 A *sphere* which rotates without slipping between two moving parallel plates

spacing $\Delta r = 2R$.

$$\omega = 2\frac{\Delta(r\Omega)}{\Delta r}$$

Therefore, in terms of derivatives,

$$\omega = 2\frac{d(r\Omega)}{dr} \tag{1}$$

Similar relationships for shear-driven systems have been indicated by simulations [38,39] and experimentally observed in 2D [40]. In our system, ω_z indeed exhibits a linear relationship with the tangential velocity gradient, as shown in Fig. 7c. Good agreement between the empirical data and a line with slope 2 indicates that gear-like motion within the shear zone may be the mechanism behind the azimuthal rotation of individual grains.

4 Discussion and conclusions

As advances in the study of granular materials continue, individual rotational motion is one aspect that is likely to receive increased attention in the near future. Measuring rotational motion experimentally brings about many difficulties, particularly for dense 3D systems of symmetric particles. To address these challenges, we have devised and performed initial experiments on the driving of drilled grains under circular split-bottom shear. The RIMS imaging technique allows us to extract the orientation of the grain cavity using PCA and measure a portion of a grain's rotational motion in 3D. While some limitations currently exist, this method has demonstrated that it is capable of making precise measurements of individual grain orientation and, in turn, rotational motion.

In particular, we can directly measure the average amount of azimuthal rotation within the shear zone, as well as investigate the potential origin of such motion. Namely, Fig. 7c indicates that rotations within the shear zone are directly coupled to the radial gradient of tangential velocity, with strong agreement between experimental data and what is theoretically predicted for a perfectly rolling system. It stands to reason, then, that varying the amount of interparticle friction would have a direct influence on shear zone size, which has previously been observed in simulations [30].

With the procedure described in this paper, one persistent limitation is that rotational motion about the drilled axis cannot be measured. In other words, the 3D images of a grain that rotates between consecutive frames entirely along the axis of the drill hole are indistinguishable. Consequently, full rotational motion of the grains cannot be captured. This limits the amount of physics that may be extracted, including locally coupled rotations, equipartition, and velocity correlations. In future studies, we will explore further modifications of the apparatus to allow us to probe full 3D rotational motion of the spheres.

Acknowledgments We would like to acknowledge helpful discussions and technical assistance from Steven Slotterback. Financial sup-

port came from the National Science Foundation (DMR0907146) and the Defense Threat Reduction Agency (HDTRA1-10-0021).

Appendix: Moments of inertia

Recall the moment of inertia for a solid sphere of mass M and radius R,

$$I_s = \frac{2}{5} M R^2$$

For the purpose of these calculations, it will be more convenient to express this in terms of density ρ,

$$I_s = \frac{8}{15} \rho \pi R^5 \tag{2}$$

First, we start with the axis along the hole, about which rotation is visually indeterminant under the current setup. For convenience, the moment of inertia of the material which is removed will be subtracted from the solid sphere inertia.

$$I_1 = I_s - I_{hole,1}$$

The moment of inertia of a differential mass element of the holed-out material is given by that of a thin solid disk,

$$\mathrm{d}I_{hole,1} = \frac{1}{2} r^2 \mathrm{d}m$$
$$\mathrm{d}I_{hole,1} = \frac{1}{2} \rho \pi r(z)^4 \mathrm{d}z,$$

where

$$r(z) = \begin{cases} h, & |z| \le \sqrt{R^2 - h^2} \\ \sqrt{R^2 - z^2}, & |z| > \sqrt{R^2 - h^2} \end{cases} \tag{3}$$

h is the hole radius in the interior of the sphere and z is the coordinate along the drill axis. Then, after performing the integrals,

$$I_1 = I_s \sqrt{1 - x^2} \left(1 + \frac{1}{2} x^2 - \frac{3}{2} x^4 \right) \tag{4}$$

In the intermediate steps, I_s is substituted in using Eq. 2 and x is defined to be the hole size ratio, $x = \frac{h}{R} < 1$. Next, we move to the moment of inertia for rotations about the axes perpendicular to the hole.

$$I_{2,3} = I_s - I_{hole,2,3}$$

We again use a thin disk as the mass element for the hole. The differential moment of inertia is then defined by applying the perpendicular and parallel axis theorems,

$$\mathrm{d}I_{hole,2,3} = \frac{1}{2} \mathrm{d}I_{hole,1} + z^2 \mathrm{d}m$$
$$\mathrm{d}I_{hole,2,3} = \frac{1}{2} \mathrm{d}I_{hole,1} + \rho \pi r(z)^2 z^2 \mathrm{d}z$$

Now, we evaluate the integrals using the same limits for z and definition of $r(z)$ from Eq. 3. Again, I_s is substituted for the solid sphere inertia and x is substituted for the hole size ratio.

$$I_{2,3} = I_s \sqrt{1 - x^2} \left(1 - \frac{3}{4} x^2 - \frac{1}{4} x^4 \right) \tag{5}$$

For our grains in particular, $\rho = 1.18\ \mathrm{g/cm^3}$. The grains have a diameter of 0.6 cm. For a solid sphere, Eq. 2 gives

$$I_s = 4.80 \cdot 10^{-3}\ \mathrm{g \cdot cm^2}$$

The hole diameter is 0.15 cm, which gives a size ratio of $x = 0.25$. From Eqs. 4 and 5,

$$I_1 = 4.77 \cdot 10^{-3}\ \mathrm{g \cdot cm^2}$$
$$I_{2,3} = 4.43 \cdot 10^{-3}\ \mathrm{g \cdot cm^2}$$

References

1. Wang, L., Frost, J., Lai, J.: Three-dimensional digital representation of granular material microstructure from x-ray tomography imaging. J. Comput. Civ. Eng. **18**, 28 (2004)
2. Nakagawa, M., Altobelli, S., Caprihan, A., Fukushima, E., Jeong, E.K.: Non-invasive measurements of granular flows by magnetic resonance imaging. Exp. Fluids **16**, 54 (1993)
3. Brujić, J., Edwards, S.F., Hopkinson, I., Makse, H.A.: Measuring the distribution of interdroplet forces in a compressed emulsion system. Physica A **327**(3–4), 201 (2003)
4. Dijksman, J.A., Rietz, F., Lőrincz, K.A., van Hecke, M., Losert, W.: Invited article: Refractive index matched scanning of dense granular materials. Rev. Sci. Instr. **83**, 011301 (2012)
5. Seidler, G.T., Martinez, G., Seeley, L.H., Kim, K.H., Behne, E.A., Zaranek, S., Chapman, B.D., Heald, S.M., Brewe, D.L.: Granule-by-granule reconstruction of a sandpile from x-ray microtomography data. Phys. Rev. E. **62**, 8175 (2000)
6. Aste, T., Saadatfar, M., Senden, T.J.: Geometrical structure of disordered sphere packings. Phys. Rev. E. **71**, 061302 (2005)
7. Zhou, J., Long, S., Wang, Q., Dinsmore, A.D.: Measurement of forces inside a three-dimensional pile of frictionless droplets. Science **312**(5780), 1631 (2006)
8. Richard, P., Philippe, P., Barbe, F., Bourlès, S., Thibault, X., Bideau, D.: Analysis by x-ray microtomography of a granular packing undergoing compaction. Phys. Rev. E. **68**, 020301 (2003)
9. Slotterback, S., Toiya, M., Goff, L., Douglas, J.F., Losert, W.: Correlation between particle motion and voronoi-cell-shape fluctuations during the compaction of granular matter. Phys. Rev. Lett. **101**, 258001 (2008)
10. Sakaie, K., Fenistein, D., Carroll, T.J., van Hecke, M., Umbanhowar, P.: Mr imaging of reynolds dilatancy in the bulk of smooth granular flows. Europhys. Lett. **84**(3), 38001 (2008)
11. Herrera, M., McCarthy, S., Slotterback, S., Cephas, E., Losert, W., Girvan, M.: Path to fracture in granular flows: dynamics of contact networks. Phys. Rev. E. **83**, 061303 (2011)
12. Börzsönyi, T., Szabó, B., Törös, G., Wegner, S., Török, J., Somfai, E., Bien, T., Stannarius, R.: Orientational order and alignment of elongated particles induced by shear. Phys. Rev. Lett. **108**, 228302 (2012)
13. Wegner, S., Börzsönyi, T., Bien, T., Rose, G., Stannarius, R.: Alignment and dynamics of elongated cylinders under shear. Soft Matter **8**, 10950 (2012)
14. Ehrichs, E.E., Jaeger, H.M., Karczmar, G.S., Knight, J.B., Kuperman, V.Y., Nagel, S.R.: Granular convection observed by magnetic resonance imaging. Science **267**(5204), 1632 (1995)

15. Huang, N., Ovarlez, G., Bertrand, F., Rodts, S., Coussot, P., Bonn, D.: Flow of wet granular materials. Phys. Rev. Lett. **94**, 028301 (2005)
16. Cheng, X., Lechman, J.B., Fernandez-Barbero, A., Grest, G.S., Jaeger, H.M., Karczmar, G.S., Möbius, M.E., Nagel, S.R.: Three-dimensional shear in granular flow. Phys. Rev. Lett. **96**, 038001 (2006)
17. Dijksman, J.A., Wandersman, E., Slotterback, S., Berardi, C.R., Updegraff, W.D., van Hecke, M., Losert, W.: From frictional to viscous behavior: three-dimensional imaging and rheology of gravitational suspensions. Phys. Rev. E. **82**, 060301 (2010)
18. Wandersman, E., Dijksman, J.A., van Hecke, M.: Particle diffusion in slow granular bulk flows. Europhys. Lett. **100**, 38006 (2012)
19. Slotterback, S., Mailman, M., Ronaszegi, K., van Hecke, M., Girvan, M., Losert, W.: Onset of irreversibility in cyclic shear of granular packings. Phys. Rev. E. **85**, 021309 (2012)
20. Hill, K.M., Caprihan, A., Kakalios, J.: Bulk segregation in rotated granular material measured by magnetic resonance imaging. Phys. Rev. Lett. **78**, 50 (1997)
21. Porion, P., Sommier, N., Faugère, A.M., Evesque, P.: Dynamics of size segregation and mixing of granular materials in a 3d-blender by nmr imaging investigation. Powder Technol. **141**(1–2), 55 (2004)
22. Harrington, M., Weijs, J.H., Losert, W.: Suppression and emergence of granular segregation under cyclic shear. Phys. Rev. Lett. **111**, 078001 (2013)
23. Nordstrom, K., Lim, E., Harrington, M., Losert, W.: Granular dynamics during impact. ArXiv e-prints (2013)
24. Jaeger, H.M., Nagel, S.R., Behringer, R.P.: Granular solids, liquids, and gases. Rev. Mod. Phys. **68**, 1259 (1996)
25. Nichol, K., Daniels, K.E.: Equipartition of rotational and translational energy in a dense granular gas. Phys. Rev. Lett. **108**, 018001 (2012)
26. Harth, K., Kornek, U., Trittel, T., Strachauer, U., Höme, S., Will, K., Stannarius, R.: Granular gases of rod-shaped grains in microgravity. Phys. Rev. Lett. **110**, 144102 (2013)
27. Brilliantov, N.V., Pöschel, T., Kranz, W.T., Zippelius, A.: Translations and rotations are correlated in granular gases. Phys. Rev. Lett. **98**, 128001 (2007)
28. Bardet, J.: Observations on the effects of particle rotations on the failure of idealized granular materials. Mech. Mater. **18**(2), 159 (1994)
29. Iwashita, K., Oda, M.: Rolling resistance at contacts in simulation of shear band development by dem. J. Eng. Mech. **124**(3), 285 (1998)
30. Luding, S.: The effect of friction on wide shear bands. Part. Sci. Tech. **26**(1), 33 (2007)
31. Halsey, T.C.: Motion of packings of frictional grains. Phys. Rev. E. **80**, 011303 (2009)
32. Oda, M., Konishi, J., Nemat-Nasser, S.: Experimental micromechanical evaluation of strength of granular materials: effects of particle rolling. Mech. Mater. **1**(4), 269 (1982)
33. Börzsönyi, T., Szabó, B., Wegner, S., Harth, K., Török, J., Somfai, E., Bien, T., Stannarius, R.: Shear-induced alignment and dynamics of elongated granular particles. Phys. Rev. E. **86**, 051304 (2012)
34. Fenistein, D., van Hecke, M.: Kinematics: wide shear zones in granular bulk flow. Nature **425**(6955), 256 (2003)
35. Fenistein, D., van de Meent, J.W., van Hecke, M.: Universal and wide shear zones in granular bulk flow. Phys. Rev. Lett. **92**, 094301 (2004)
36. Tsai, J.C., Gollub, J.P.: Slowly sheared dense granular flows: crystallization and nonunique final states. Phys. Rev. E. **70**(3), 031303 (2004)
37. Crocker, J.C., Grier, D.G.: Methods of digital video microscopy for colloidal studies. J. Colloid. Interf. Sci. **179**, 298 (1996)
38. Lun, C.K.K., Bent, A.A.: Numerical simulation of inelastic frictional spheres in simple shear flow. J. Fluid Mech. **258**, 335 (1994)
39. da Cruz, F., Emam, S., Prochnow, M., Roux, J.N.: Rheophysics of dense granular materials: Discrete simulation of plane shear flows. Phys. Rev. E. **72**, 021309 (2005)
40. Zhang, J., Behringer, R.P., Goldhirsch, I.: Coarse-graining of a physical granular system. Prog. Theor. Phys. Suppl. **184**, 16 (2010)